Research Article

Suchandra Banerjee*, Russell Chipman, Nathan Hagen and Yukitoshi Otani

Native oxide layer effect on polarization cancellation for mirrors over the visible to near-infrared region

https://doi.org/10.1515/aot-2020-0004
Received January 22, 2020; accepted March 10, 2020

Abstract: The presence of native oxide layers on aluminum mirrors can be a nuisance for precision optical design. As the native oxide thickness varies from mirror to mirror, its effect cannot be completely canceled even in the conventional crossed fold mirror geometry. We show how this effect arises and how it can be mitigated, and provide an experimental demonstration in which the residual linear retardance and linear diattenuation are reduced to <0.14° and <0.001, respectively, over the visible and near-infrared spectral range.

Keywords: Mueller matrix polarimeter; oxide layer; polarization; polarization ray tracing.

1 Introduction

Mirrors are considered as ideal reflectors when they reflect 100% of light such that Fresnel amplitude reflection coefficients for s and p polarization $r_s = r_p = 1$ for all angles of incidence. For metal mirrors, however, r_s and r_p are not equal. An amplitude and a phase difference between r_s and r_p appear as linear diattenuation and linear retardance. These make the reflectance polarization dependent. Breckinridge et al. show that fold mirrors have more impact on induced polarization than the primary and secondary mirrors of a Cassegrain telescope have. This induced polarization varies with the angle of incidence and the material property of reflecting elements [1, 2].

The induced polarization can be measured with a polarimeter. Optical instruments like telescopes, spectrometers, and imaging systems are combined with the polarimeters to retrieve polarization information of various objects. Shamir et al. [3] analyze the effect of induced polarization in an optical system and show that it is necessary to eliminate this effect for an accurate polarization measurement.

Clark et al. [4] show how to mitigate the induced polarization using a spatially varying retardance plate. However, this method requires a complicated fabrication process, needs several stacks of birefringent plates, and is limited to controlling only linear retardance. Mahler et al. [5] proposed an optical system design where linear diattenuation is kept below 1% by designing the system's mirror coatings.

In an optical system sensitive to polarization effects, uncapped mirrors are the norm, in order to minimize the effect of multilayer coatings on the polarization state. Many laboratory experiments are done over UV to near-infra-red region, and uncapped aluminum mirrors are used, which show more than 90% of average reflectance. Capped mirrors are generally designed for a particular spectrum band. Lam et al. [6, 7] reported that both of the linear retardance and linear diattenuation can be balanced simultaneously using a crossed fold mirror configuration. Gold mirrors were selected for their simulation, which showed high performance only in the infra-red region.

Aluminum coatings have less polarization sensitivity than silver and gold, and they are common due to their high reflectivity over UV to near-infra-red wavelength range and its high thermal resistivity [2, 8]. However, unlike gold, aluminum reacts with oxygen when exposed to air and forms a thin native oxide layer on the top of the surface. The presence of oxide changes the polarization properties (linear retardance and linear diattenuation) of the mirror [9]. Harten et al. [10] studied the growth of

***Corresponding author: Suchandra Banerjee,** Graduate School of Engineering, Utsunomiya University, Utsunomiya, Tochigi 321-8585, Japan, e-mail: banerjee.suchandra@gmail.com
Russell Chipman: College of Optical Sciences, University of Arizona, Tucson, AZ 85721, USA
Nathan Hagen and Yukitoshi Otani: Department of Optical Engineering, Center for Optical Research and Education, Utsunomiya University, Utsunomiya, Tochigi 321-8585, Japan

www.degruyter.com/aot

Published online April 17, 2020

oxide layer after evaporation for a long time and showed the saturation time of the oxidation of a real aluminum mirror. Depending on environment conditions, the saturation level of thin native oxide layer may vary from mirror to mirror [10, 11].

A broadband achromatic tunable polarization rotator was proposed over visible to near-infra-red spectrum using three uncapped aluminum mirrors to make the whole system more cost effective than using capped mirrors [12]. The experimental results confirmed that even after polarization cancellation using crossed fold mirror geometry, a residual amount of linear retardance was present, which increased the system's overall linear retardance.

In this manuscript, we show the impact of native oxide layer thickness on linear retardance and linear diattenuation by modeling thin films of Al_2O_3 on the top of the aluminum. Native oxide layer thicknesses are determined by fitting the measured linear retardance spectrum to a Fresnel reflection model. In order to demonstrate the effect of the native oxide layer on the polarization, we measure the polarization of a beam reflected by pairs of crossed fold mirrors and compare the results with no oxide layers, determined by theory. We verify the effect of native oxide layers on polarization cancellation by a Mueller matrix spectro-polarimeter over the wavelength range 500–800 nm. The extent of polarization cancellation is shown for different oxide layer thicknesses.

2 Determination of aluminum mirror's polarization properties in the presence of oxide layers

Figure 1 shows the behavior of *s* and *p* polarizations upon reflection from an ideal reflector, a bare aluminum reflector, and a real aluminum reflector. Light experiences multiple reflections between the thin oxide and aluminum layers. A relative phase shift ϕ occurs between the air-oxide and the oxide-aluminum interfaces and is expressed as

$$\phi = \frac{2\pi}{\lambda} n_1 d \cos i_0, \tag{1}$$

with the oxide layer thickness d for the wavelength of light λ and refractive index n_1 [13] of the oxide layer. The amplitude reflection coefficients for *s*- and *p*-polarized light can be found by coherently summing all of the partially reflected beams' reflection coefficients and are written as

$$r_s = \frac{r_{01s} + r_{12s} e^{i\phi}}{1 + r_{01s} r_{12s} e^{i\phi}} = \rho_s e^{i\Phi_s},\ r_p = \frac{r_{01p} + r_{12p} e^{i\phi}}{1 + r_{01p} r_{12p} e^{i\phi}} = \rho_p e^{i\Phi_p}, \tag{2}$$

where r_{01} and r_{12} are the Fresnel reflection coefficients for medium 0 to 1 and for medium 1 to 2, respectively. The overall amplitude for the *s* and *p* components are denoted by ρ_s and ρ_p, and Φ_s and Φ_p are the overall phase parts of Eq. (2). For aluminum, the fast axis is along the direction of the *s*-polarized light. Linear retardance δ_F and linear diattenuation D_F of the real aluminum mirror are calculated using amplitude reflection coefficients [Eq. (2)] as

$$\delta_F = \Phi_s - \Phi_p,\ D_F = (|r_s|^2 - |r_p|^2)/(|r_s|^2 + |r_p|^2). \tag{3}$$

Using Eqs. (1–3), it is evident that the polarization parameters δ_F and D_F are functions of thickness of the oxide layer d. These are plotted in Figure 2 as a function of wavelength for varying oxide layer thicknesses at 45° angle of incidence. The linear retardances in Figure 2 include the geometrical transformation effect, which occurs due to odd number reflections where a $\pm\pi$ phase shift is introduced at each reflection. If we remove the geometrical transformation effect (by subtracting 180°) in Figure 2, we find that the linear retardance actually increases with the physical thickness of the oxide layer for the VNIR wavelength range. The effect of the oxide layer on linear diattenuation is less apparent but cannot be ignored for high-accuracy polarization measurements. The induced polarizations of a one-aluminum fold mirror can be balanced by orienting another aluminum fold

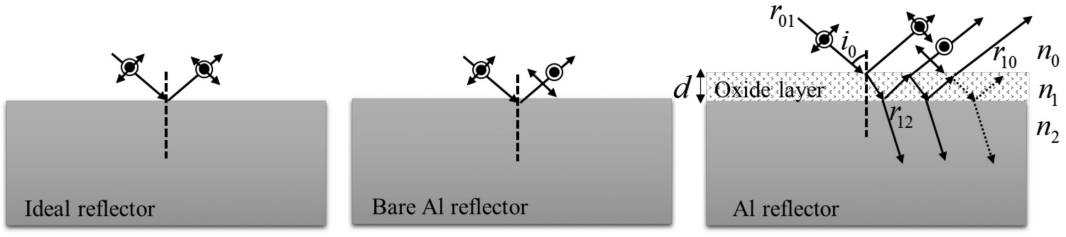

Figure 1: Behavior of *s* and *p* polarization components upon reflection from (A) an ideal reflector, (B) a bare aluminum reflector (aluminum without native oxide layer), and (C) a real aluminum reflector (aluminum with native oxide layer).

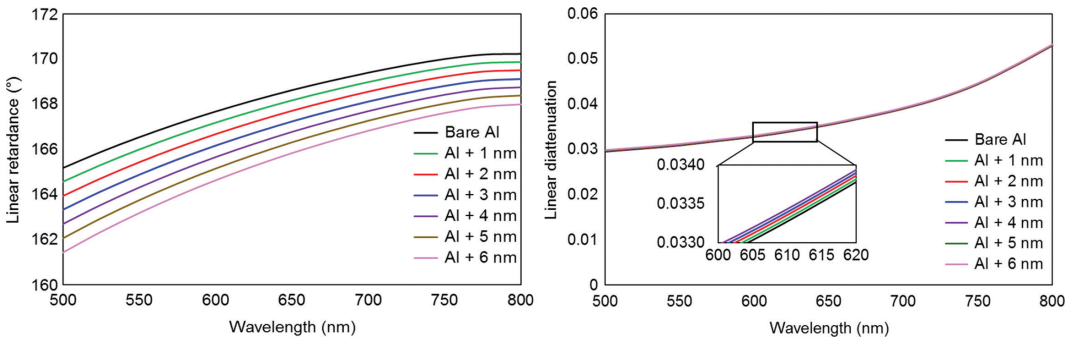

Figure 2: The effect of oxide layer thickness on polarization parameters: linear retardance and diattenuation. Both δ_F and D_F are plotted as a function of wavelength in the VNIR region for oxide layer thicknesses from 1 to 6 nm.

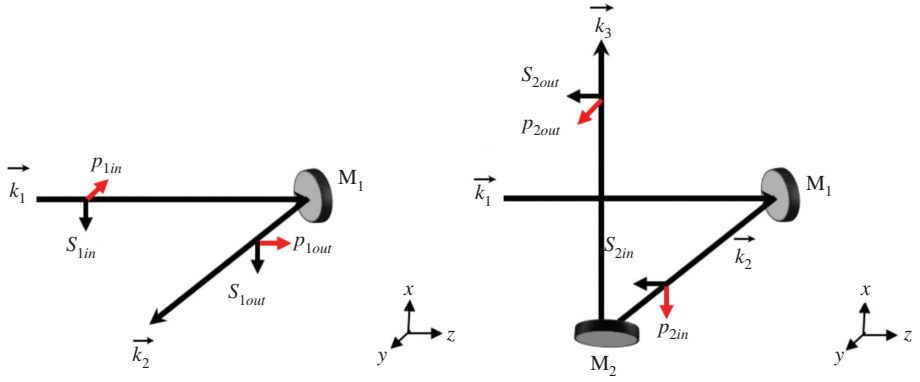

Figure 3: The *s* and *p* polarization transformations through (A) the first mirror M_1 along light direction $\mathbf{k}_1$ and $\mathbf{k}_2$ and (B) the crossed fold mirror geometry.

mirror's surface normal in such a way that the fast polarization axis of the first mirror is transformed into the slow polarization axis of the second mirror and vice versa. This is called the *crossed fold mirror* (CFM) geometry [6]. Here, the linear diattenuation of the second fold mirror takes an opposite sign of the first mirror's, so that linear diattenuation and linear retardance both cancel out [7].

For the CFM geometry, let us define the propagation vectors as

$$\mathbf{k}_1 = \{0, 0, 1\}, \mathbf{k}_2 = \{0, 1, 0\}, \mathbf{k}_3 = \{1, 0, 0\}. \quad (4)$$

Incident light propagates along the *z* direction until the first mirror M_1 and gets reflected along the *y* direction until it meets the second mirror M_2. After reflection from M_2, the light exits along the *x* direction. The **s**, **p**, and **k** are mutually orthogonal to each other, therefore for each mirror surface, **s** and **p** polarization vectors can be found as

$$\begin{aligned}\mathbf{s}_{q,\text{in}} &= \mathbf{s}_{q,\text{out}} = (\mathbf{k}_q \times \mathbf{n}_{q+1})/|\mathbf{k}_q \times \mathbf{n}_{q+1}|,\\ \mathbf{p}_{q,\text{in}} &= (\mathbf{k}_q \times \mathbf{s}_{q,\text{in}})/|\mathbf{k}_q \times \mathbf{s}_{q,\text{in}}|, \mathbf{p}_{q,\text{out}}\\ &= (\mathbf{k}_{q+1} \times \mathbf{s}_{q,\text{out}})/|\mathbf{k}_{q+1} \times \mathbf{s}_{q,\text{out}}|,\end{aligned} \quad (5)$$

where $q \in \{1,2\}$ represents the mirror's number. For *q*th mirror, the phase ϕ_q is associated with oxide layer thickness d_q. Polarization transformation through CFM geometry is shown in Figure 3. The direction $\mathbf{k}_q$ of ray propagation is determined by the mirror's surface normal vector $\mathbf{n}_q$ as

$$\mathbf{n}_q = (\mathbf{k}_q - \mathbf{k}_{q+1})/|\mathbf{k}_q - \mathbf{k}_{q+1}|. \quad (6)$$

Using Eqs. (4–6), it is seen in Table 1 that the fast axis of the first mirror along $\mathbf{s}_{1,\text{in}}$ is transformed into the slow axis of the second mirror along $\mathbf{p}_{2,\text{in}}$, and the slow axis of

Table 1: Crossed fold mirror geometry: mirror surface orientation (n_q), input *s*-polarization direction ($\mathbf{s}_{q,\text{in}}$), and incident and exiting *p*-polarization directions ($\mathbf{p}_{q,\text{in}}$ and $\mathbf{p}_{q,\text{out}}$).

$\mathbf{n}_1$	$\mathbf{S}_{1,\text{in}}$	$\mathbf{p}_{1,\text{in}}$	$\mathbf{p}_{1,\text{out}}$
$\{0, -1/\sqrt{2}, 1/\sqrt{2}\}$	$\{-1, 0, 0\}$	$\{0, -1, 0\}$	$\{0, 0, 1\}$
$\mathbf{n}_2$	$\mathbf{s}_{2,\text{in}}$	$\mathbf{p}_{2,\text{in}}$	$\mathbf{p}_{2,\text{out}}$
$\{-1/\sqrt{2}, 1/\sqrt{2}, 0\}$	$\{0, 0, -1\}$	$\{-1, 0, 0\}$	$\{0, 1, 0\}$

the first mirror, which is along $\mathbf{p}_{1,\text{out}}$, becomes the fast axis of the second mirror along $\mathbf{s}_{2,\text{in}}$.

To quantify the linear retardance and the linear diattenuation after polarization cancellation, we use a polarization ray tracing (PRT) matrix calculus model of the CFM configuration [14]. The PRT matrix $\mathbf{P}_q$ is a modified form of Jones matrix in local coordinates $\{s, p\}$, projected into the global $\{s, p, k\}$ coordinate system. The linear retardance and linear diattenuation of the CFM configuration cannot be determined by simply cascading individual Jones matrices of reflecting surfaces. Hence, the PRT matrix calculation method is used to determine the polarization behavior for such a system. As $\mathbf{s}$, $\mathbf{p}$, and $\mathbf{k}$ are orthogonal to each other, they form an orthogonal matrix $\mathbf{O}_q$. By relating the augmented Jones matrix of the mirror with the input and output orthogonal matrices $\mathbf{O}_{q,\text{in}}$ and $\mathbf{O}_{q,\text{out}}$, the PRT matrix $\mathbf{P}_q$ is formed as

$$\begin{aligned}\mathbf{P}_q &= \mathbf{O}_{q,\text{out}}\mathbf{J}_q\mathbf{O}_{q,\text{in}}^{-1} \\ &= \begin{pmatrix} s_{q,x} & p_{q+1,x} & k_{q+1,x} \\ s_{q,y} & p_{q+1,y} & k_{q+1,y} \\ s_{q,z} & p_{q+1,z} & k_{q+1,z} \end{pmatrix} \begin{pmatrix} r_s & 0 & 0 \\ 0 & r_p & 0 \\ 0 & 0 & 1 \end{pmatrix} \begin{pmatrix} s_{q,x} & p_{q,x} & k_{q,x} \\ s_{q,y} & p_{q,y} & k_{q,y} \\ s_{q,z} & p_{q,z} & k_{q,z} \end{pmatrix}^{-1}, \end{aligned} \tag{7}$$

where $\mathbf{s}_q$ and $\mathbf{p}_q$ are given in Eq. (5). The matrix $\mathbf{P}_q$ includes the geometrical transformation effect, which makes an incident right-handed coordinate system into a left-handed coordinate system upon reflection. The $\mathbf{Q}_q$ matrix does not contain any polarization information and purely depends on the $\{\mathbf{s}, \mathbf{p}, \mathbf{k}\}$ coordinate system. By multiplying the reflection matrix $\mathbf{I}$ with the input and output orthogonal matrices ($\mathbf{O}_{q,\text{in}}$ and $\mathbf{O}_{q,\text{out}}$), the geometrical transformation matrix $\mathbf{Q}$ for surface number q is

$$\begin{aligned}\mathbf{Q}_q &= \mathbf{O}_{q,\text{out}}\mathbf{I}\mathbf{O}_{q,\text{in}}^{-1} \\ &= \begin{pmatrix} s_{q,x} & p_{q+1,x} & k_{q+1,x} \\ s_{q,y} & p_{q+1,y} & k_{q+1,y} \\ s_{q,z} & p_{q+1,z} & k_{q+1,z} \end{pmatrix} \begin{pmatrix} 1 & 0 & 0 \\ 0 & -1 & 0 \\ 0 & 0 & 1 \end{pmatrix} \begin{pmatrix} s_{q,x} & p_{q,x} & k_{q,x} \\ s_{q,y} & p_{q,y} & k_{q,y} \\ s_{q,z} & p_{q,z} & k_{q,z} \end{pmatrix}^{-1}. \end{aligned} \tag{8}$$

To eliminate the inversion effect due to an odd number of reflections, an inverse geometrical transformation matrix $\mathbf{Q}_q$ is applied on $\mathbf{P}_q$, and $\mathbf{Q}_q^{-1}\mathbf{P}_q$ is obtained. The cumulative $\mathbf{P}$ and $\mathbf{Q}$ matrices for the CFM system (Figure 3) are given by

$$\mathbf{P} = \mathbf{P}_2\mathbf{P}_1, \text{ and } \mathbf{Q} = \mathbf{Q}_2\mathbf{Q}_1. \tag{9}$$

We determine the linear retardance δ and linear diattenuation D of pairs of mirrors in the CFM geometry from a singular value decomposition of $\mathbf{Q}^{-1}\mathbf{P}$, which gives Unitary and diagonal matrices in the form $\mathbf{U}\sum\mathbf{V}$. Linear retardance is the difference between fast and slow polarization axes λ_f and λ_s of the Unitary matrix, which is written as

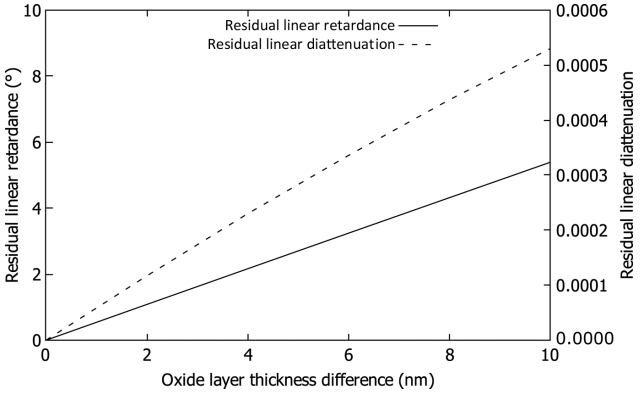

Figure 4: Effect of oxide layer thickness difference on residual linear retardance and diattenuation of the crossed fold mirror configuration.

$$\delta = \arg[\lambda_f] - \arg[\lambda_s]. \tag{10}$$

The diagonal matrix has singular values (t_f and t_s), which correspond to the magnitude of reflection coefficients r_s and r_p. Thus, D can be formulated as

$$D = \frac{t_f^{\,2} - t_s^{\,2}}{t_f^{\,2} + t_s^{\,2}}. \tag{11}$$

The amount of linear retardance and linear diattenuation [Eqs. (10) and (11)] for the CFM configuration depends on the oxide layer thicknesses d_1 and d_2. If the oxide layer thicknesses are not perfectly equal to each other, there will be a residual amount of linear retardance and diattenuation even after cancellation. This is shown in Figure 4 where the polarization cancellation is not perfectly balanced due to having $d_1 \neq d_2$ and leaves a residue.

3 System and methods

For our experiments, we employ a dual rotating retarder-based spectroscopic Mueller matrix polarimeter (Axometrics, Huntsville, AL, USA) [https://www.axometrics.com/products/axoscan]. The polarimeter configuration is based on Azzam's model [15]. The Axometrics polarimeter (ASMP) has mainly four units: light source, polarization state generator (PSG), polarization state analyzer (PSA), and detector. The light source is a tunable visible Xenon arc lamp (500–800 nm) in ASMP. The PSG and PSA are free to move and can be set manually to any desired position. We retrieve sample polarization characteristics, namely, retardance, diattenuation, and depolarization by decomposing the full Mueller matrix using the Lu-Chipman

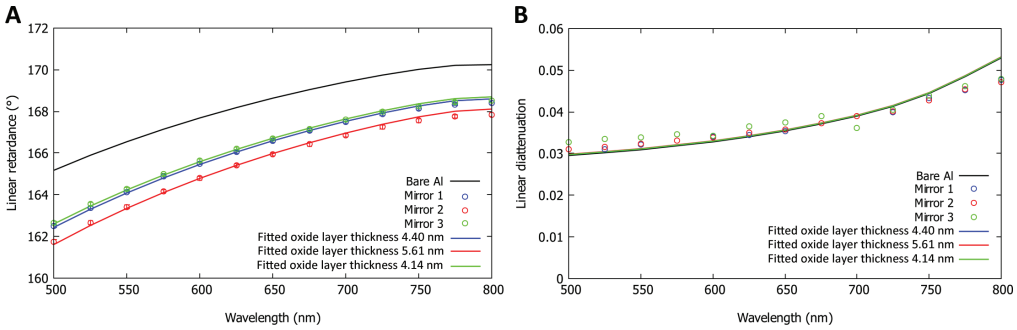

Figure 5: Spectroscopic measurement of polarization of three aluminum mirrors at a 45° angle of incidence: (A) measured linear retardance and (B) linear diattenuation are fitted with oxide layer thicknesses using Eqs. (1–3).

method [16, 17]. The system's accuracy is verified first by measuring air as a sample. The ASMP system has an accuracy of 0.1% and has a precision of 0.01% in the Mueller matrix elements for 40 points of averaging data together. After decomposing the Mueller matrix, the maximum error present in linear retardance is 0.01° and in diattenuation is 0.001 in the VNIR range.

4 Experimental results and discussion

We measure the polarization characteristics of three aluminum flat mirrors M_1, M_2, and M_3 (TFAN-10C03-10, Global Optosigma) at 45° angle of incidence by ASMP. Aluminum mirrors without thin film coating are selected for the measurement. All of the mirrors are kept in room temperature for more than 180 days such that the oxide layer thickness has stabilized. The surface normal of the mirrors are set at 45° and are placed in a mechanical stage having a precision of 0.01°. Three mirrors are then placed one at a time in between the PSG and PSA of the ASMP, and the Mueller matrix is measured to retrieve the complete polarization characteristics.

Figure 5 shows the measured linear retardance and diattenuation of the mirrors over the VNIR. It is observed from Figure 5 that the linear retardance values are different for the three mirrors, although the mirrors have the same aluminum coating [18]. Also, the linear retardance values of M_1, M_2, and M_3 are not equal with the simulated linear retardance of a bare aluminum mirror. The measurements are repeated five times with 40 average points, and the maximum error present in linear retardance is ±0.08° (Figure 5A). The mismatch in linear retardance between bare aluminum and the measured real aluminum mirrors is because of the native oxide layer. The oxide layer thicknesses are determined by fitting the measured linear retardance data using Eqs. (1–3). After fitting the linear retardance data spectrally over 500–800 nm, the amount of native oxide layer thicknesses are determined as 4.40 ± 0.15 nm, 5.61 ± 0.19 nm, and 4.14 ± 0.15 nm, respectively, for M_1, M_2, and M_3. With these native oxide layer thicknesses, diattenuation is also fitted over the spectrum and is shown in Figure 5B. Next, we perform polarization cancellation by choosing two different sets of mirrors depending on their native oxide layer thickness separation. The first pair M_1-M_2 and second pair M_1-M_3

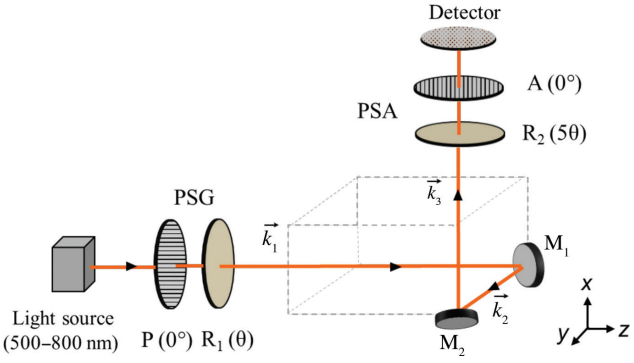

Figure 6: The experimental setup for measurement of polarization cancellation: P, polarizer; R, retarder; A, analyzer are used in a Mueller matrix polarimeter. Rotation angles of retarders are θ and 5θ, respectively, in the PSG and PSA. M_1-M_2 is arranged according to propagation directions (k). The laboratory coordinate system is shown.

have native oxide layer thickness differences of 1.21 nm and 0.26 nm, respectively. Each pair of mirrors is placed in the CFM configuration in between the PSG and PSA of the ASMP following the propagation directions given in Eq. (4). Figure 6 shows the experimental layout. The Mueller matrix of the mirror pair is measured over a spectrum. The residual linear retardance and linear diattenuation are retrieved using the Lu-Chipman decomposition method, with results shown in Figure 7. We perform five successive measurements to determine the error and are shown in Figure 7. It is observed that both of the polarization parameters (δ and D) are close to perfectly balanced when the native oxide layer thickness difference is minimized. For the first pair of mirrors having 1.21 nm of native oxide layer thickness difference, there is a residual linear retardance of 0.65 ± 0.01° and linear diattenuation of 0.003 at 650 nm. For the second pair of mirrors having almost equal oxide layer thicknesses (different by only 0.26 nm), the residual linear retardance and linear diattenuation reduce to 0.14 ± 0.02° and 0.001 at 650 nm, as shown in Figure 7.

If polarization cancellation is exactly balanced, the magnitudes of the diagonal elements of the Mueller matrix for the mirror pair become one, while the non-diagonal elements are zero. For a non-ideal mirror pair, the polarization cancellation, which is shown over the spectral range 500–800 nm (Figure 7), the polarization compensation is almost constant over the specified spectrum region. This is

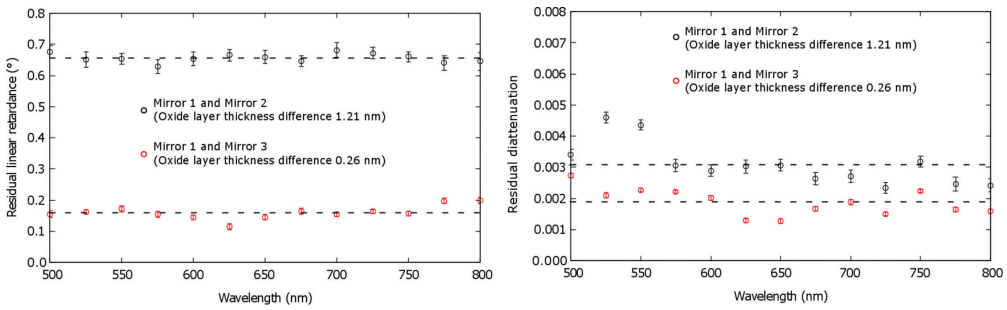

Figure 7: Decomposed linear retardance and diattenuation after polarization cancellation using the CFM configuration. Both δ and D shrink with smaller difference of oxide layer thicknesses. The dotted line shows the theoretical value after cancellation.

expected from the nature of the measured linear retardance data of the three mirrors (Figure 5).

When polarized light reflects from a rough surface, light gets scattered, and the degree of polarization of the incident polarized light reduces. So to confirm the roughness of the aluminum thin film, we measure the depolarization parameter from a 4×4 Mueller matrix, which shows a value almost equal to the System's error level (0.001). Thus, it ensures the roughness of the top surface of the mirror. The roughness influences the depolarization parameter only and does not have any impact on the linear retardance and diattenuation.

5 Conclusion

We presented the polarization behavior of environment-sensitive aluminum mirrors when a natural oxidation forms, and then, we showed how this native oxide layer causes artifacts on polarization balancing using various sets of the CFM configurations. First, we determine the amount of native oxide layer thickness from the polarization properties of the aluminum mirrors over the VNIR. The oxide layer thickness varies from mirror to mirror, as we confirmed by measuring linear retardance of three aluminum fold mirrors (M_1, M_2, and M_3). Next, we performed polarization cancellation using the CFM geometry. We showed and demonstrated experimentally using an ASMP how the oxide layer thickness differences determine a system's polarization sensitivity. We showed that polarization cancellation is getting closer to perfectly balanced when cross fold mirrors have almost equal native oxide layer thicknesses.

A system's sensitivity determines how much residual δ and D can be tolerated. High-precision optical systems like micro-lithography, lenses, coronagraphs, and space-borne telescopes require high accuracy measurements, so that the polarization needs to be controlled to the tolerance level of a system.

In theory, a batch of mirrors are all processed in the same way, exposed to the same coating source for the same length of time, and then to the same oxygenated atmosphere, giving them identical coating properties. In real manufacturing environments, there exist variations in mirror properties even within the same batch. The measurement of the oxide layer, thus, can be useful for chirped mirrors or optical elements in telescopes to cancel unwanted effects of manufacturing uncertainty.

For real telescopic and other optical systems, polarization cancellation needs to perform across a set of rays, and analysis is necessary to do over the exit pupil. In such cases, the native oxide layer thickness variation over the surface may effect on the predicted behavior, and thus, we are extending this analysis from point detection measurement to imaging across the full diameter of the fold mirror and will be shown in a future publication.

Acknowledgment: S. Banerjee is grateful to the Ministry of Education Culture, Sports, Science and Technology—Government of Japan (MEXT) for a supporting scholarship.

References

[1] J. B. Breckinridge, W. S. T. Lam and R. A. Chipman, PSAP 127, 445–468 (2015).
[2] J. Zhang, X. Zhang, S. Tan and X. Xie, Curr. Opt. Photon 1, 364–371 (2017).
[3] J. Shamir and R. A. Chipman, J. Mod. Opt. 38, 327–347 (1991).
[4] N. Clark and J. B. Breckenridge, Proc. SPIE 8146 (2011).
[5] A. B. Mahler, P. K. Smith and R. A. Chipman, Proc. SPIE 6682 (2007).
[6] W. S. T. Lam and R. Chipman, Appl. Opt. 54, 3236–3245 (2015).
[7] P. W. Maymon and R. A. Chipman. Opt. Photonics 1746, 148–156 (1992).
[8] Y. Yang and C. Yan, Appl. Opt. 55, 1343–1350 (2016).
[9] D. M. Harrington, S. R. Sueoka and A. J. White, J. Astron. Telesc. Instrum. Syst. 3 (2017).

[10] G. van Harten, F. Snik and C. U. Keller, Publ. Astron. Soc. Pac 121, 377–383 (2009).
[11] G. Hass and N. W. Scott, J. Phys. Radium 11, 394–402 (1950).
[12] S. Banerjee, R. Chipman, N. Hagen and Y. Otani, Opt. Commun. 454, 124456 (2020).
[13] H. Malitson and M. J. Dodge, J. Opt. Soc. Am. 62, 1405 (1972).
[14] G. Yun, S. C. McClain and R. A. Chipman, Appl. Opt. 50, 2866–2874 (2011).
[15] R. M. A. Azzam, Opt. Lett. 2, 148–150 (1978).
[16] D. H. Goldstein, Appl. Opt. 31, 6676–6683, (1992).
[17] S. Y. Lu and R. A. Chipman, J. Opt. Soc. Am. A 13, 1106–1113 (1996).
[18] K. M. McPeak, S. V. Jayanti, S. J. P. Kress, S. Meyer, S. Iotti, et al., ACS Photonics 2, 326–333 (2015).